SYSTEMATIC AND MULTI-CRITERIA OPTIMISATION OF SUBCRITICAL THERMALLY INTEGRATED CARNOT BATTERIES (TI-PTES) IN AN EXTENDED DOMAIN

Antoine Laterre[1,2,*], Olivier Dumont[2], Vincent Lemort[2], Francesco Contino[1]

[1] *Thermodynamics and Fluid Mechanics, Institute of Mechanics, Materials and Civil Engineering, Université catholique de Louvain, Place du Levant 2, 1348 Louvain-la-Neuve, Belgium*
[2] *Thermodynamics Laboratory, Aerospace and Mechanical Engineering Department, University of Liège, Allée de la Découverte 17, 4000 Liège, Belgium*

*Corresponding Author: antoine.laterre@uclouvain.be

ABSTRACT

Thermally integrated pumped thermal energy storage (TI-PTES) is a flexibility option to recover low-grade heat (i.e. < 100°C) and to provide overnight storage. Common criteria when optimising such system are the power-to-power efficiency (i.e. electricity recovery), the total exergy efficiency (i.e. combined heat and electricity recovery) and the energy density (i.e. storage size). However, these objectives are generally conflicting and multi-criteria optimisation is therefore required to discuss the trade-offs. Design guidelines have been proposed for some specific case studies but are still lacking for the remaining wide range of possible integration scenarios. This work therefore presents a systematic multi-criteria analysis of a TI-PTES consisting of a high temperature vapor compression heat pump, a sensible heat thermal storage and an organic Rankine cycle, in an extended integration domain (i.e. heat source from −25 to 100°C, sink from −25 to 50°C). The single objective optimisation reveals that the design trends are not uniform and that the tipping points are located where the difference between the source and sink temperatures is less than 30 K. The multi-criteria analysis shows that there is a region of the domain where the criteria do not conflict. The results also highlight that density and exergy efficiency are much less conflicting with each other than they are with power-to-power efficiency.

1 INTRODUCTION

Next to sobriety measures, improving the efficiency of energy systems and supporting the integration of renewables are key elements of the energy transition. This includes the deployment of flexibility options, such as energy storage, as well as reducing the amount of energy lost in conversion from one form to another. In this regard, it has been estimated that in 2012, 52 % of the primary energy consumed worldwide was actually lost as so-called recoverable waste heat (Forman *et al.*, 2016). Despite its reduced exergy (i.e. 63 % of this waste energy had a temperature below 100°C, which is corresponds to only 21 % of the total waste heat exergy content), the challenges of energy transition cannot waste any piece of the enormous volume of energy consumed every year.
There exist several routes for waste heat recovery, such as exergy upgrade with high temperature vapor compression heat pumps (HT-VCHP) and conversion to electricity with organic Rankine cycles (ORC). However, there is not always an on-site thermal demand, and the waste heat can have too low exergy potential to be directly converted into electricity. In such case, thermally integrated pumped thermal energy storage (TI-PTES, or Carnot batteries) could be another option (Frate *et al.*, 2017). Indeed, TI-PTES can increase the efficiency of renewable energy systems through waste heat recovery, while providing the necessary flexibility (i.e. energy storage).
Since its first mentions (Mercangöz *et al.*, 2012; Steinmann, 2014) and actual first characterisation (Frate *et al.*, 2017), the concept has attracted growing interest and several implementations have been proposed. The most common is the basic hot TI-PTES layout (see Fig. 1), consisting in a subcritical HT-VCHP, a two-tank sensible thermal energy storage (TES) and a subcritical ORC.

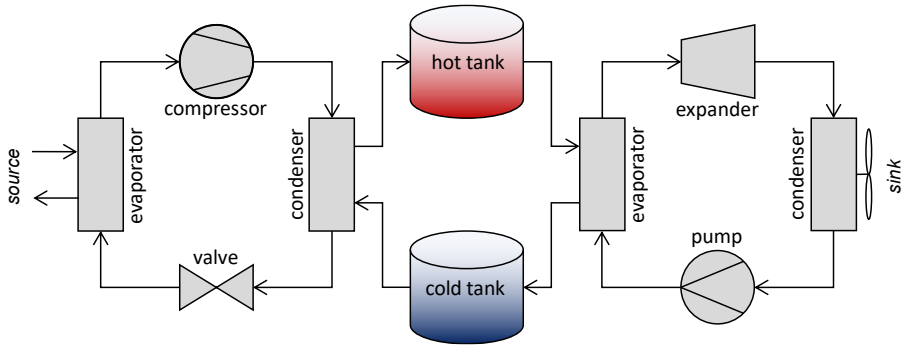

Figure 1: Cycle layout of the basic hot TI-PTES. Note that the circulating pumps are not considered.

When optimising the thermodynamic cycle of these storage systems, typical criteria are to maximise the power-to-power efficiency η_{P2P} (i.e. efficiency of electricity recovery), the total exergy efficiency η_{II} (i.e. efficiency of combined heat and electricity recovery) and the electrical energy density ρ_{el} (i.e. storage size). However, as pointed out by Frate *et al.* (2020a), these three objectives can be conflicting. This implies that it is not possible to design a TI-PTES system that maximises these criteria simultaneously, and that trade-offs must therefore be discussed. Recently, it has been suggested to formalise this conflicting nature by referring to it as the *Carnot battery trilemma* (Weitzer *et al.*, 2022a).

For now, many studies have optimised the thermodynamic design of TI-PTES and proposed cycle modifications to enhance some performance indicators, like η_{P2P} (e.g. internal regenerators (Frate *et al.*, 2020a), organic flash cycles (Weitzer *et al.*, 2022b), zeotropic mixtures (Lu *et al.*, 2022), …). On the other hand, far fewer have focused on optimising and mapping the performance of TI-PTES with respect to the *Carnot battery trilemma* in the entire thermal integration domain (i.e. combination of possible source and sink temperatures). As an illustration, the current domain exploration for TI-PTES with sensible TES is represented in Fig. 2. It can be observed that the region with source temperatures below 60°C has been particularly little explored. This can be attributed in part to the fact that, due to Carnot efficiency, η_{P2P} is lower in that region of the domain (i.e. usually below 50 %), whereas as TI-PTES has often been considered primarily as an electrical storage option, this performance may have seemed rather poor. However, when looking at TI-PTES as a flexible waste heat recovery option, there is no indication that η_{P2P} should override η_{II}. Moreover, a significant share (i.e. 45 %) of the low temperature waste heat to be recovered (i.e. < 200°C) is precisely below 60°C, as shown by Marina *et al.* (2021).
A direct consequence of this poor investigation of the integration domain is that it is currently not possible to provide theoretical maximum performance and design guidelines for TI-PTES across the entire domain, and with regard to the three criteria of the *Carnot battery trilemma*.

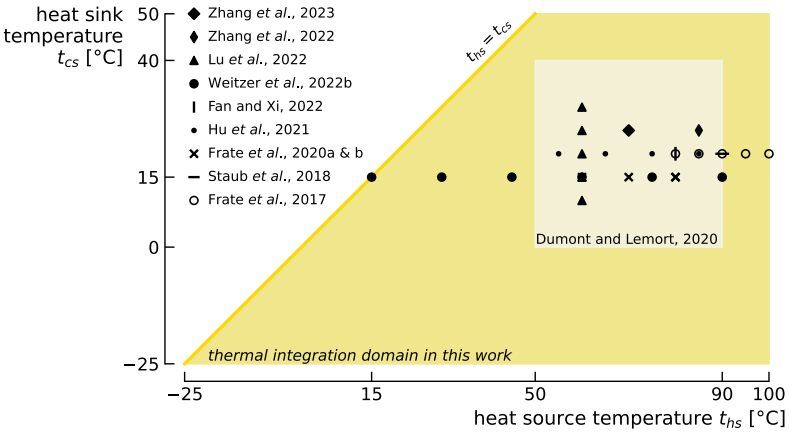

Figure 2: Current exploration of the thermal integration domain for TI-PTES with sensible TES. Note that most authors have not studied the *Carnot battery trilemma* in its entirety.

The goal of this work is therefore to investigate and characterise the *Carnot battery trilemma* in the entire integration domain, with ambient temperatures ranging from -25 to $50°C$ to cover the majority of climates that can be encountered (i.e. from polar to dry). More precisely, an optimisation of the basic hot TI-PTES cycle is first conducted to maximise separately each objective of the *trilemma*. The idea is to map the maximum theoretical performance that could be reached and to formulate design guidelines according to the desired objectives. The results are used to assess whether the guidelines can be generalised to the whole domain or whether they need to be adapted in each region. A specificity of the method is to simultaneously optimise the thermodynamic cycle and the choice of working fluids, to fully embrace the potential synergies between them. Then, a multi-criteria optimisation is proposed to characterise the *trilemma* in the entire domain. Based on the results, implementation constraints are discussed, and design recommendations and cycle improvements are finally proposed.

2 METHODOLOGY

2.1 System description

The system investigated in this work is the basic hot TI-PTES. The latter consists in a subcritical HT-VCHP, a two-tank pressurized water TES and a subcritical air-cooled ORC (see Fig. 1). Although enhanced cycles give better performance, the basic configuration is adopted as the aim of this study is to provide generic design guidelines. Based on the obtained results, cycle improvements are suggested in the last section. The two-tank architecture is preferred to a single tank as it provides a constant thermal profile regardless of the state of charge and storage duration (i.e. no diffusion losses due to a thermocline). However, assuming a perfect thermocline, the results obtained here can extrapolate to the single tank case (Frate *et al.*, 2020a).

The thermodynamic performance of the system is assessed using an in-house `Python` model[1]. The corresponding model parameters are summarised in Table 1. `CoolProp` is used to access the fluids properties (Bell *et al.*, 2014). In the model, the evaporation and condensation pressures are obtained with a pinch analysis. Also note that the thermal storage losses are neglected (i.e. overnight storage). Finally, the heat source and sink are treated as dry atmospheric air (i.e. only sensible heat is considered).

2.2 Optimisation problem

The *Carnot battery trilemma* consists of the trade-off between the power-to-power efficiency η_{P2P}, the exergy efficiency η_{II}, and the energy density ρ_{el}. These performance indicators are therefore adopted for the single objective and multi-criteria optimisations. They are defined as

$$\eta_{P2P} = \frac{W_{orc}}{W_{hp}} \quad (1) \qquad \eta_{II} = \frac{W_{orc}}{W_{hp}+Ex_{hs}} \quad (2) \qquad \rho_{el} = \frac{h_{st,ht}-h_{st,lt}}{v_{st,ht}+v_{st,lt}} \cdot \eta_{orc} \quad (3)$$

where W_{orc} and W_{hp} are the ORC and HT-VCHP net power output and input respectively, and Ex_{hs} is the exergy of the heat source. The reference state used for the latter's definition corresponds to the heat sink temperature, so $t_{hs} = t_{cs}$ yields $\eta_{II} = \eta_{P2P}$. The density is defined as the ratio between the difference in specific enthalpy of the tanks and their specific volumes, multiplied by the ORC efficiency.

To optimise the performance of TI-PTES, a set of eight design variables are used. The hot tank storage temperature $t_{st,ht}$, the heat source glide $\Delta T_{hs,gl}$ and the storage temperature spread $\Delta T_{st,sp}$ (i.e. the temperature difference between the hot and cold tanks) have already been identified as key parameters influencing η_{P2P}, η_{II} and ρ_{el} respectively (Dumont and Lemort, 2020; Frate *et al.*, 2020a; Weitzer *et al.*, 2022b). Note that it is here assumed that the heat source can be treated as free waste heat (i.e. $\Delta T_{hs,gl}$ has no constrained value and is therefore used as a design variable). We also include the liquid subcooling $\Delta T_{hp,sc}$ in the HT-VCHP as well as the vapor superheat $\Delta T_{hp/orc,sh}$ in the HT-VCHP and in the ORC. Indeed, these parameters can take different optimum values depending on the thermal profiles and working fluids (Frate *et al.*, 2020a; Maraver *et al.*, 2014). The constraints associated with these variables are reported in Table 1.

[1] The code can be provided upon request.

Table 1: Model parameters and constraints for the TI-PTES optimisation.

Name	Symbol	Value	Name	Symbol	Value
Heat source temperature	t_{hs}	-25 to 100°C	Heat sink temperature	t_{cs}	-25 to 50°C
Heat source temp. glide	$\Delta T_{hs,gl}$	*design var.*	Heat sink temp. glide	$\Delta T_{cs,gl}$	10 K [(b)]
HP vapor superheat	$\Delta T_{hp,sh}$	*design var.*	ORC vapor superheat	$\Delta T_{orc,sh}$	*design var.*
HP liquid subcooling	$\Delta T_{hp,sc}$	*design var.*	ORC liquid subcooling	$\Delta T_{orc,sc}$	3 K [(c)]
Min. HP temperature lift	$\Delta T_{hp,min}$	5 K [(a)]	Min. ORC temp. drop	$\Delta T_{orc,min}$	5 K [(a)]
HP working fluid	$fluid_{hp}$	*design var.*	ORC working fluid	$fluid_{orc}$	*design var.*
Compressor efficiency	$\eta_{is,comp}$	0.75 [(a)]	Expander efficiency	$\eta_{is,exp}$	0.75 [(a)]
Max. compress. exit temp.	$t_{comp,max}$	180°C [(b)]	Pump efficiency	$\eta_{is,pmp}$	0.50 [(a)]
Min. HP/ORC superheat	$\Delta T_{sh,min}$	3 K [(c)]	Min. HP subcooling	$\Delta T_{sc,min}$	3 K [(c)]
Hot tank storage temp.	$t_{st,ht}$	*design var.*	Storage temp. spread	$\Delta T_{st,sp}$	*design var.*
Max. storage temperature	$t_{st,ht,max}$	150°C [(c)]	Storage pressure	p_{st}	7.5 bar
Min. storage temperature	$t_{st,lt,min}$	$t_{hs} - \Delta T_{hs,gl}$	Min. HP/ORC pressure	$p_{hp/orc,min}$	0.5 bar [(b)]
Pinch point in exchangers	ΔT_{pp}	3 K [(a,b)]	Pressure losses	Δp	0.0 bar [(b,c)]

[(a)] Dumont and Lemort, 2020 [(b)] Frate *et al.*, 2020a [(c)] Weitzer *et al.*, 2022a

Finally, an innovation of the method proposed here is to simultaneously optimise the thermodynamic cycle and the selection of working fluids in the HT-VCHP and ORC, to fully embrace the potential synergies between them. A set of 31 working fluids are used. These were selected from the list of those available in `CoolProp` because they have a zero ODP, a low GWP and because their critical point is compatible with the range of temperatures investigated in this work (i.e. thermal domain and storage temperatures). These fluids are available in Table A1 in Appendix.

To map the performance of TI-PTES, the integration domain is discretised with a 5 K resolution into 296 cells. Both single objective and multi-criteria optimisations are then carried out using NSGA-II (Deb *et al.*, 2002) through the `RHEIA` framework (Coppitters *et al.*, 2022). In order to guarantee a sufficient domain exploration, the population size is set to 500 and the mutation probability to 50 %. Note that this probability is very high, which leaves room for improvement in future work. Since no formal convergence criteria exists in NSGA-II, the minimum number of generations is set to 800. However, in many of the cells, much more generations have been run to get satisfactory results.

3 RESULTS

3.1 Single objective optimisation

The three optimisations have been conducted separately in the extended integration domain to maximise η_{P2P}, η_{II}, and ρ_{el}, respectively. The obtained mappings are depicted in Fig. 3. They are represented as a payoff table to illustrate the conflict between the different objectives of the *trilemma*. The corresponding design variables are depicted in Fig. 5. For the sake of brevity, the optimum vapor superheat and liquid subcooling in the HT-VCHP and ORC, as well as the optimum selection of working fluids, are not reported in this paper. They will be discussed in future work.

Results for optimised η_{P2P}

The power-to-power efficiency increases with the difference between the source and sink temperatures ΔT_{hs-cs} from about 25 % when $\Delta T_{hs-cs} = 0$ K to about 320 % when $\Delta T_{hs-cs} = 125$ K. However, because of a design shift, the growth is not continuous (i.e. the tipping point is $\Delta T_{hs-cs} = 30$ K). Indeed, for $\Delta T_{hs-cs} > 30$ K, $t_{st,ht}$ is minimised (i.e. the heat pump lift is always 5 K, its minimum value), so the coefficient of performance of the heat pump is maximised. Instead, for $\Delta T_{hs-cs} \leq 30$ K, $t_{st,ht}$ gradually increases with decreasing ΔT_{hs-cs}. The existence of this tipping point, which had already been detected by Weitzer *et al.* (2022b) and Jockenhöfer *et al.* (2018), can be explained with η_{P2P}^{Carnot}, the Carnot efficiency of TI-PTES (i.e. the thermodynamic limit). Considering the irreversibilities at the heat exchanges, which can be modelled as the temperature difference ΔT between the fluids, the latter

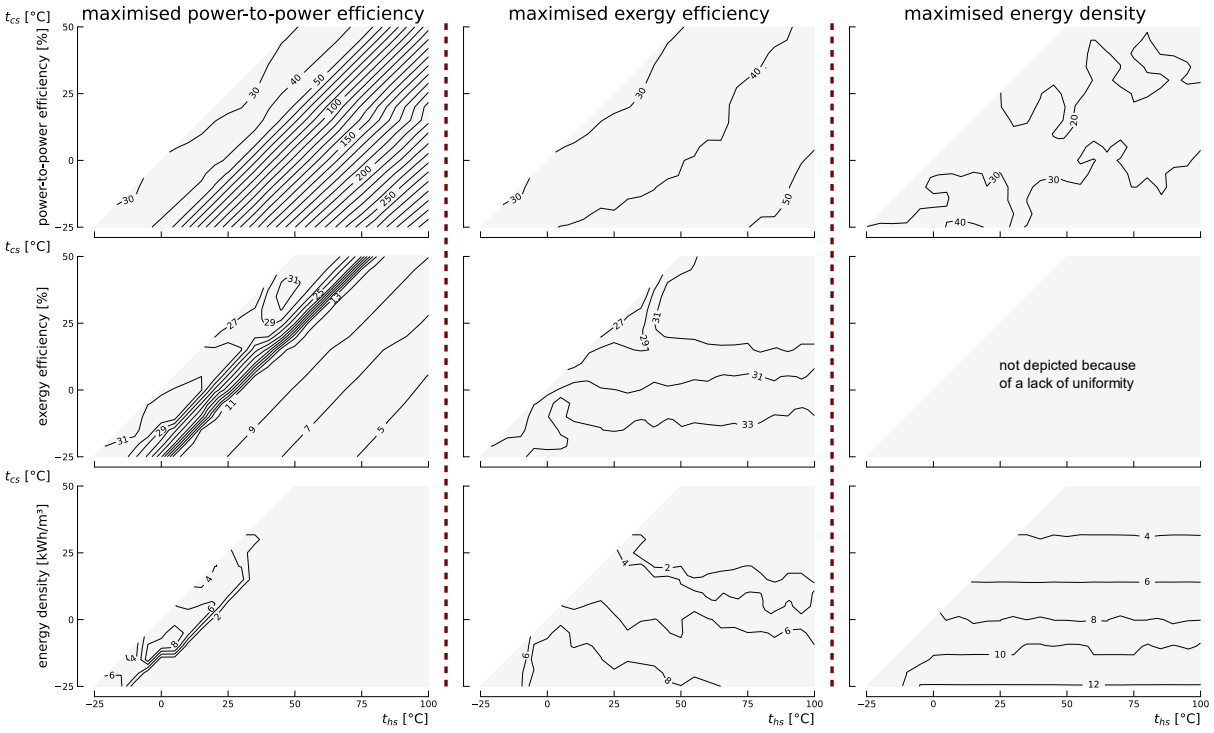

Figure 3: Payoff table with η_{P2P} (1st row), η_{II} (2nd row) and ρ_{el} (3rd row) for the configurations maximising η_{P2P} (1st column), η_{II} (2nd column) and ρ_{el} (3rd column) respectively. Some contour lines have been smoothed to eliminate local convergence issues (model artefacts).

is defined as

$$\eta_{P2P}^{Carnot} = COP_{HT-VCHP}^{Carnot} \cdot \eta_{ORC}^{Carnot} = \frac{(t_{st,ht}+\Delta T)(t_{st,ht}-t_{cs}-2\cdot\Delta T)}{(t_{st,ht}-\Delta T)(t_{st,ht}-t_{hs}+2\cdot\Delta T)} \quad , \qquad (4)$$

and it is depicted in Fig. 4 for different $t_{st,ht}$, ΔT and ΔT_{hs-cs}. When ΔT_{hs-cs} is below the tipping point (i.e. < 30 K), the exergy losses at the ORC cannot be sufficiently compensated by the high COP, thus $t_{st,ht}$ must be increased to reduce these losses, so that the resulting η_{P2P} is improved (see Fig. 4a). Please note, however, that this analysis with the Carnot efficiency is somewhat incomplete since it suggests maximising $t_{st,ht}$ to maximise η_{P2P}, while an optimal $t_{st,ht}$ actually exists, as observed in Fig. 5 (i.e. there exist optimum trade-offs between $COP_{HT-VCHP}$ and η_{orc}).
It can also be shown that the greater the irreversibilities in heat transfers (i.e. the greater ΔT), the higher the tipping point. Note that the particular case $\Delta T = 0$ (i.e. no irreversibilities) does not allow detection of the tipping point, and therefore leads to incorrect conclusions about the optimum $t_{st,ht}$ (see Fig. 4b).

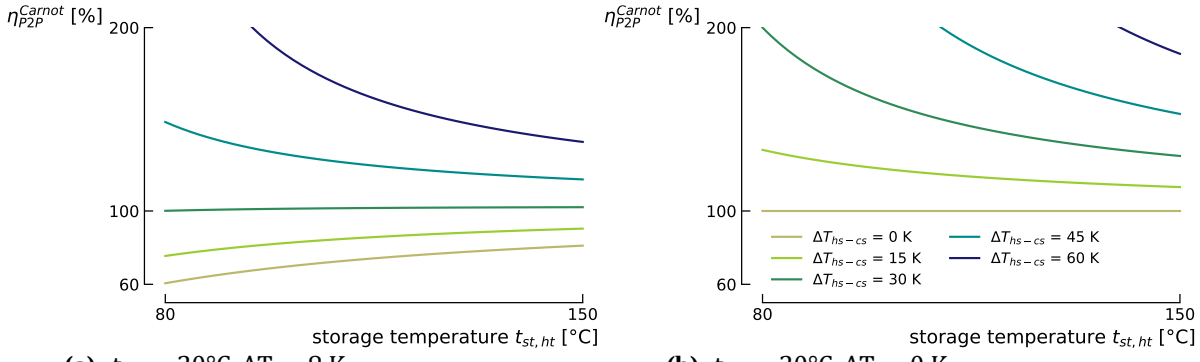

(a) $t_{cs} = 20°C, \Delta T = 8$ K **(b)** $t_{cs} = 20°C, \Delta T = 0$ K

Figure 4: Carnot efficiency of TI-PTES with and without consideration of heat transfer irreversibilities. The latter are represented through ΔT, the temperature difference between the fluids.

Ultimately, these results illustrate that, when ΔT_{hs-cs} is above the tipping point, the search for the maximum η_{P2P} leads to a TI-PTES degenerated into a TES + ORC (i.e. the heat pump lift is minimised), which makes it a waste heat recovery option, but no longer a true electrical storage system.

Regarding the other two design variables, since maximising η_{P2P} involves getting as close as possible to ideal Carnot cycles, $\Delta T_{st,sp}$ and $\Delta T_{hs,gl}$ are minimised on the largest part of the domain to limit the exergy losses at the heat transfers. However, there exists a narrow region (i.e. $\Delta T_{hs-cs} < 20$ K and $t_{hs} \leq 25°C$) where $t_{st,ht}$ is maximised and $\Delta T_{st,sp}$ takes much higher values: there, the relative storage spread, which is defined as

$$\Delta T_{st,sp}^{rel} = \frac{\Delta T_{st,sp}}{t_{st,ht} - t_{hs}} \quad , \qquad (5)$$

is approximately 60 %. Interestingly, this leads to increased η_{II} and ρ_{el}, what relaxes the *Carnot battery trilemma*, as this will be further discussed in the multicriteria analysis.

Results for optimised η_{II}

The exergy efficiency drops with t_{cs} from about 35 % when $t_{cs} = -25°C$ to about 30 % when $t_{cs} = 15°C$, mainly due to the reduction in W_{orc}. In that region of the domain, $t_{st,ht}$ is always maximised (i.e. maximisation of W_{orc} to the cost of increased W_{hp}) and $\Delta T_{st,sp}$ is between 60 and 100 K (i.e. relative decrease in W_{hp} due to increased cooling effect, thanks to larger subcooling at the condenser). This result is partly in contrast with that of Frate *et al.* (2020a) who, for equivalent design variables, also recommended maximising $t_{st,ht}$ but minimising $\Delta T_{st,sp}$. Sensitivity analyses will be conducted in future works to better understand the role of $\Delta T_{st,sp}$ w.r.t. the imposed design constraints.

When $t_{cs} > 15°C$, η_{II} slightly re-increases and stabilises around 32 % because of a design shift: $t_{st,ht}$ and $\Delta T_{st,sp}$ are reduced to about 130°C (especially for lower ΔT_{hs-cs}) and 10 K respectively. The reason for this shift will be further explored in future works but could be due to a limited fluid availability when $t_{cs} < 15°C$ (i.e. high critical point required while respecting the minimum pressure constraint).

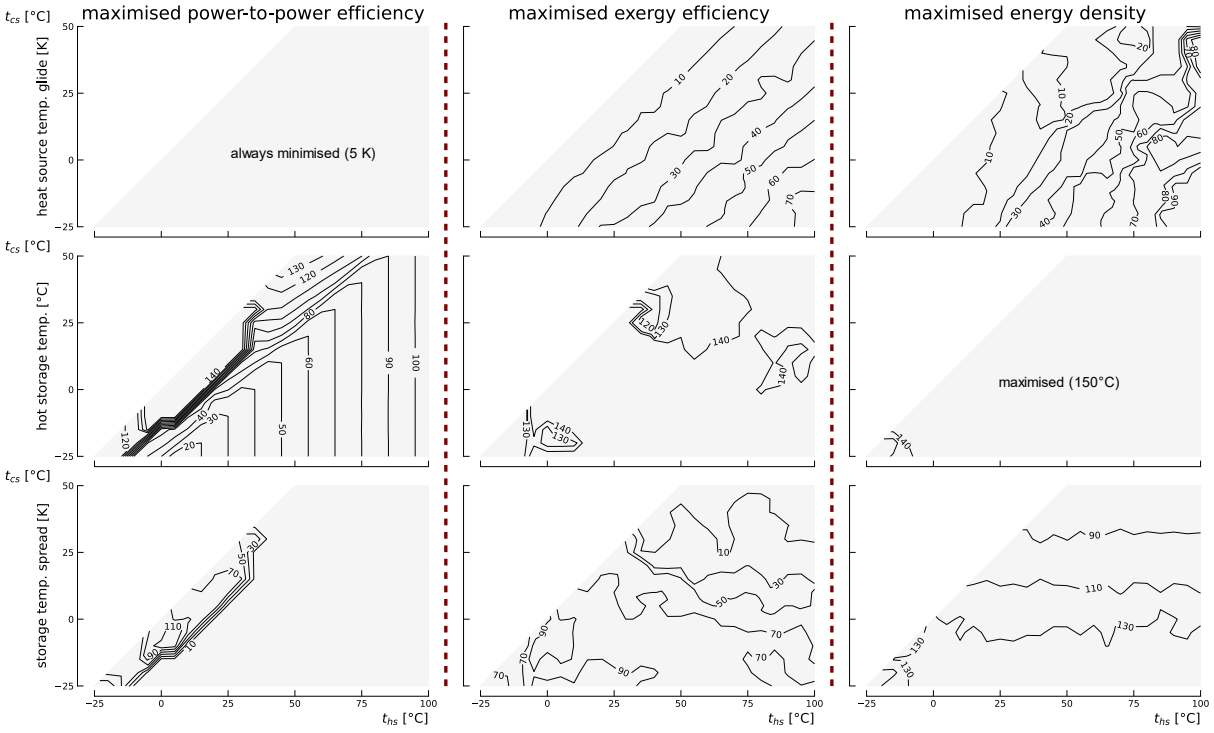

Figure 5: Set of design variables with the most significant influence on the *Carnot battery trilemma*: $\Delta T_{hs,gl}$ (1st row), $t_{st,ht}$ (2nd row) and $\Delta T_{st,sp}$ (3rd row). Some contour lines have been smoothed to eliminate local convergence issues (model artefacts).

The other key parameter influencing η_{II} is $\Delta T_{hs,gl}$. A high $\Delta T_{hs,gl}$ leads to an effective waste heat utilisation but reduces $COP_{HT-VCHP}$ as the evaporation temperature is decreased. A trade-off must therefore be found. A relevant result of this study is that the relative heat source glide, defined as

$$\Delta T_{hs,gl}^{rel} = \frac{\Delta T_{hs,gl}}{\Delta T_{hs-cs}} \quad , \quad (6)$$

must always be comprised between 55 and 60 % in order to maximise η_{II}.
Let's finally observe that η_{II} is always superior for TI-PTES than in other power-to-x-to-power systems, which hardly exceed 25 % (Dias *et al.*, 2020). Note that this does not consider the waste heat that is lost when the TI-PTES is not charging.

Results for optimised ρ_{el}
The optimum electrical energy density results of a trade-off between the thermal density (i.e. the higher $\Delta T_{st,sp}$, the higher the thermal density) and η_{orc} (i.e. the higher $\Delta T_{st,sp}$, the lower η_{orc}). As it can be observed in Fig. 3, because η_{orc} is a function of t_{cs}, ρ_{el} linearly decreases with increasing t_{cs}. It ranges from 12.1 kWh/m^3 when $t_{cs} = -25°C$ to 2.5 kWh/m^3 when $t_{cs} = 50°C$. Note that a thermal storage in a single tank with an ideal thermocline could double these values, as one of the two tanks would be removed.
The optimum storage spread linearly varies from around 145 K when $t_{cs} = -25°C$ to 72 K when $t_{cs} = 50°C$. To reach such spreads and to maximise η_{orc}, $t_{st,ht}$ is always maximised. Moreover, as a rule of thumb, it can be shown that for designs maximising the density, $t_{st,ht} - t_{cs} - \Delta T_{st,sp} \approx 27$ K.
Note that although $\Delta T_{hs,gl}$ takes a certain trend with ΔT_{hs-cs}, there is still a lack of convergence. This is due to the fact that this parameter does not have a direct influence on ρ_{el}, but it must have a sufficient value for $t_{st,lt}$ to be higher than $t_{hs} - \Delta T_{hs,gl}$ (see constraint in Table 1).

Finally, in a general way for all the results, it is observed that when $t_{hs} \leq -20°C$, the optimised designs are not in total agreement with what has been described above (i.e. they have lower $t_{st,ht}$ and $\Delta T_{st,sp}$). This is due to the constraint on $p_{hp/orc,min}$, which imposes to choose fluids with lower critical points, as they have higher saturation pressures at lower temperatures, and to the subcritical regime constraint.

3.2 Multi-criteria analyses

The Pareto fronts obtained with the multi-criteria analyses are shown for two locations of the domain in Fig. 6. These fronts are used to draw qualitative trends exclusively, the quantitative results being specific to each position in the integration domain. To quantify the conflict between the three objectives, a criterion has been established using the best and worst performance as follows:

$$i_{conflict} = \sqrt{\frac{\left(\frac{\eta_{P2P}^{max} - \eta_{P2P}^{min}}{\eta_{P2P}^{max}}\right)^2 + \left(\frac{\eta_{II}^{max} - \eta_{II}^{min}}{\eta_{II}^{max}}\right)^2 + \left(\frac{\rho_{el}^{max} - \rho_{el}^{min}}{\rho_{el}^{max}}\right)^2}{3}} \quad . \quad (7)$$

The thresholds to discriminate the different areas on the map are set arbitrarily. When $i_{conflict} \leq 15$ %, the conflict is said to be slight. For $15\ \% < i_{conflict} \leq 50\ \%$, it is medium. Above, it is high. Fig. 6a shows that the criteria are only slightly conflicting for $t_{hs} = 25°C$ and $t_{cs} = 15°C$. Indeed, the relative difference between the best and worst performance is only 1.9 % for η_{P2P}, 1.7 % for η_{II} and 3.2 % for ρ_{el}. In general, this result can be extended to the whole region of the domain where $t_{hs} \leq 25°C$ and $\Delta T_{hs-cs} < 20$ K, as the relative difference between the best and worst performance of each criterion does not usually exceed 15 % (see light grey zone in Fig. 6).
In contrast, Fig. 6b shows that the *trilemma* is much more intense for $t_{hs} = 55°C$ and $t_{cs} = 15°C$. The front between η_{P2P} and η_{II} is linear, and it results mainly of a simultaneous trade-off between $\Delta T_{hs,gl}$, $t_{st,ht}$ and $\Delta T_{st,sp}$, which in line with the observations drawn in the previous section. The steep front between ρ_{el} and η_{P2P} illustrates well the very binary nature of the problem: it is not really possible to obtain a satisfactory trade-off between the two criteria, as one tends to clearly degrade the other. Indeed,

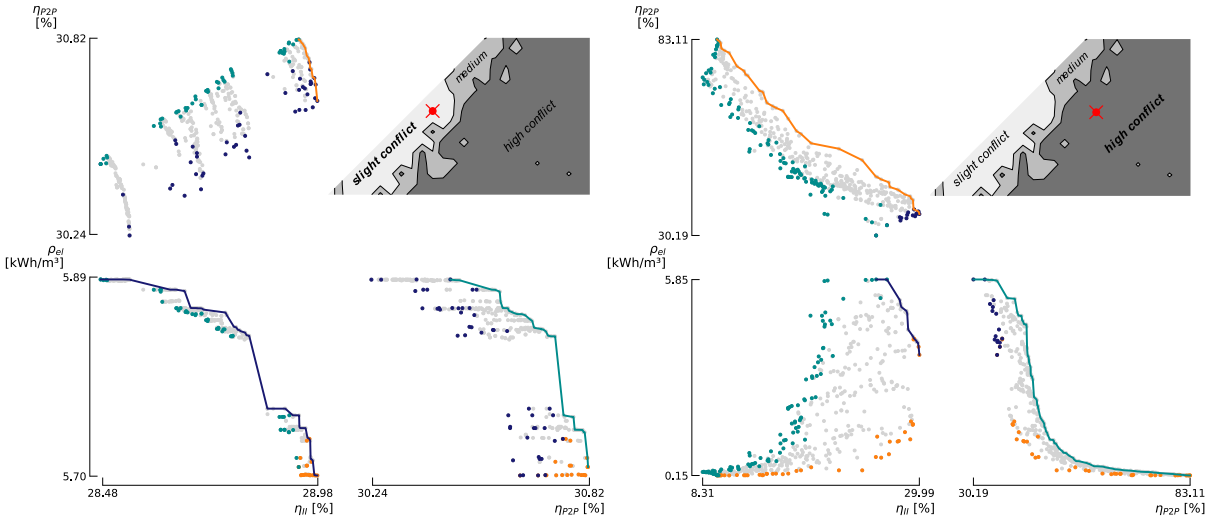

(a) 25°C heat source and 15°C heat sink ($\Delta T_{hs-cs} = 10$ K)

(b) 55°C heat source and 15°C heat sink ($\Delta T_{hs-cs} = 40$ K)

Figure 6: 3D Pareto fronts of the *Carnot battery trilemma* for two locations in the integration domain. The map of the domain shows the conflict between the three criteria.

the maximisation of η_{P2P} requires minimising $\Delta T_{hs,gl}$, $t_{st,ht}$ and $\Delta T_{st,sp}$ whereas opposite trends are observed for ρ_{el}. Finally, it can be noted that ρ_{el} and η_{II} are much less conflicting with each other than with η_{P2P}. This is largely due to the fact that they both maximise $t_{st,ht}$ over most of the domain, and that they do not minimise $\Delta T_{st,sp}$ and $\Delta T_{hs,gl}$.

4 CONCLUSION AND DISCUSSIONS

This work focused on the analysis of the *Carnot battery trilemma* over the entire thermal integration domain. The objectives were to map the theoretical performance that TI-PTES could reach, to formulate design guidelines and to study the conflict between η_{P2P}, η_{II} and ρ_{el}.
It was found that, when optimised, η_{P2P} is a function of ΔT_{hs-cs}, and that η_{II} and ρ_{el} are functions of t_{cs} only. Moreover, it has been shown that, for each objective, general design guidelines can be established. Yet, it has also been demonstrated that, for the considered set of design constraints, these guidelines are not uniform across the domain and that the existence of tipping points lead to the formation of sub-regions. This applies in particular to $t_{st,ht}$ and $\Delta T_{st,sp}$ when optimising η_{P2P} and η_{II}.
The multi-criteria analysis also revealed the existence of a region where the three objectives are almost not conflicting. This means that the *trilemma* does not have the same intensity over the whole thermal domain. In general, the main source of conflict is the value of $t_{st,ht}$, which must be minimised to maximise η_{P2P} and maximised to maximise η_{II} and ρ_{el}.

According to the results obtained, improvements could be made to the basic TI-PTES. Firstly, when the HT-VCHP lift is very high, the required compression ratio can exceed 30. This suggests the use of multistage or cascaded heat pumps. Then, for designs involving large $\Delta T_{st,sp}$, two cases can be encountered. In the first, the evaporation point in the ORC is relatively low compared to the critical point, with a possible vapor superheat (e.g. maximisation of η_{II}). In such case, the use of an internal regenerator could be interesting. Nevertheless, this consideration depends on the choice of the fluid and deserves further investigation. In the second case, the ORC operates very close to the critical point, with a potentially large superheat. This highlights that the use of transcritical ORCs could be relevant in such configurations. Finally, the presence of important glides should push towards further investigation of the use of zeotropic mixtures. Some of these points will be addressed in future work, together with more detailed analyses of the designs, including the choice of fluids, and the role of liquid subcooling and vapor superheat.

NOMENCLATURE

Abbreviations

COP	coefficient of performance	ORC	organic Rankine cycle
GWP	global warming potential	TES	thermal energy storage
HT-VCHP	high temperature vapor compression heat pump	TI-PTES	thermally integrated pumped thermal energy storage
ODP	ozone depletion potential		

Greek and Latin letters

ΔT	temperature difference, K	p	pressure, bar
Δp	pressure loss, bar	ρ	density, kWh/m^3
η	efficiency, %	t	temperature, °C
h	specific enthalpy, J/kg/K	v	specific volume, m^3/kg

Sub- and superscript

cs	cold sink	II	exergy
el	electrical	lt	low temperature
gl	temperature glide	P2P	power-to-power
hp	heat pump	pp	pinch point
hs	hot source	rel	relative
hs − cs	source – sink temperature	sp	spread
ht	high temperature	st	storage

REFERENCES

Bell, I.H., Wronski, J., Quoilin, S., Lemort, V., 2014. Pure and pseudo-pure fluid thermophysical property evaluation and the open-source thermophysical property library CoolProp. *Industrial & engineering chemistry research* 53, 2498–2508.

Coppitters, D., Tsirikoglou, P., Paepe, W.D., Kyprianidis, K., Kalfas, A., Contino, F., 2022. RHEIA: Robust design optimization of renewable Hydrogen and dErIved energy cArrier systems. *Journal of Open Source Software* 7, 4370.

Deb, K., Pratap, A., Agarwal, S., Meyarivan, T., 2002. A fast and elitist multiobjective genetic algorithm: NSGA-II. *IEEE transactions on evolutionary computation* 6, 182–197.

Dias, V., Pochet, M., Contino, F., Jeanmart, H., 2020. Energy and economic costs of chemical storage. *Frontiers in Mechanical Engineering* 6, 21.

Dumont, O., Lemort, V., 2020. Mapping of performance of pumped thermal energy storage (Carnot battery) using waste heat recovery. *Energy* 211, 118963.

Fan, R., Xi, H., 2022. Energy, exergy, economic (3E) analysis, optimization and comparison of different Carnot battery systems for energy storage. *Energy Conversion and Management* 252, 115037.

Forman, C., Muritala, I.K., Pardemann, R., Meyer, B., 2016. Estimating the global waste heat potential. *Renewable and Sustainable Energy Reviews* 57, 1568–1579.

Frate, G.F., Antonelli, M., Desideri, U., 2017. A novel Pumped Thermal Electricity Storage (PTES) system with thermal integration. *Applied Thermal Engineering* 121, 1051–1058.

Frate, G.F., Ferrari, L., Desideri, U., 2020a. Multi-criteria investigation of a pumped thermal electricity storage (PTES) system with thermal integration and sensible heat storage. *Energy Conversion and Management* 208, 112530.

Frate, G.F., Ferrari, L., Desideri, U., 2020b. Multi-Criteria Economic Analysis of a Pumped Thermal Electricity Storage (PTES) With Thermal Integration. *Front. Energy Res.* 8, 53.

Hu, S., Yang, Z., Li, J., Duan, Y., 2021. Thermo-economic analysis of the pumped thermal energy storage with thermal integration in different application scenarios. *Energy Conversion and Management* 236, 114072.

Jockenhöfer, H., Steinmann, W.-D., Bauer, D., 2018. Detailed numerical investigation of a pumped thermal energy storage with low temperature heat integration. *Energy* 145, 665–676.

Lu, P., Luo, X., Wang, J., Chen, J., Liang, Y., Yang, Z., He, J., Wang, C., Chen, Y., 2022. Thermodynamic analysis and evaluation of a novel composition adjustable Carnot battery under variable operating scenarios. *Energy Conversion and Management* 269, 116117.

Maraver, D., Royo, J., Lemort, V., Quoilin, S., 2014. Systematic optimization of subcritical and transcritical organic Rankine cycles (ORCs) constrained by technical parameters in multiple applications. *Applied Energy* 117, 11–29.

Marina, A., Spoelstra, S., Zondag, H.A., Wemmers, A.K., 2021. An estimation of the European industrial heat pump market potential. *Renewable and Sustainable Energy Reviews* 139, 110545.

Mercangöz, M., Hemrle, J., Kaufmann, L., Z'Graggen, A., Ohler, C., 2012. Electrothermal energy storage with transcritical CO2 cycles. *Energy* 45, 407–415.

Smith, C., Nicholls, Z.R.J., Armour, K., Collins, W., Forster, P., Meinshausen, M., Palmer, M.D., Watanabe, M., 2021. The Earth's Energy Budget, Climate Feedbacks, and Climate Sensitivity Supplementary Material. Climate Change 2021: The Physical Science Basis. Contribution of Working Group I to the Sixth Assessment Report of the Intergovernmental Panel on Climate Change.

Steinmann, W.D., 2014. The CHEST (Compressed Heat Energy STorage) concept for facility scale thermo mechanical energy storage. *Energy* 69, 543–552.

Weitzer, M., Müller, D., Karl, J., 2022a. Two-phase expansion processes in heat pump – ORC systems (Carnot batteries) with volumetric machines for enhanced off-design efficiency. *Renewable Energy* 199, 720–732.

Weitzer, M., Müller, D., Steger, D., Charalampidis, A., Karellas, S., Karl, J., 2022b. Organic flash cycles in Rankine-based Carnot batteries with large storage temperature spreads. *Energy Conversion and Management* 255, 115323.

Zhang, M., Shi, L., Hu, P., Pei, G., Shu, G., 2023. Carnot battery system integrated with low-grade waste heat recovery: Toward high energy storage efficiency. *Journal of Energy Storage* 57, 106234.

Zhang, Y., Xu, L., Li, J., Zhang, L., Yuan, Z., 2022. Technical and economic evaluation, comparison and optimization of a Carnot battery with two different layouts. *Journal of Energy Storage* 55, 105583.

ACKNOWLEDGEMENTS

The first author acknowledges the support of Fonds de la Recherche Scientifique - FNRS [40014566 FRIA-B1]. The computational resources have been provided by the Consortium des Équipements de Calcul Intensif (CÉCI), funded by the Fonds de la Recherche Scientifique de Belgique (F.R.S.-FNRS) under Grant No. 2.5020.11 and by the Walloon Region.

APPENDIX

Table A1: Technical and physical properties of the investigated working fluids (data from `CoolProp 6.4.1` (Bell *et al.*, 2014)).

Fluid	Category	T_{crit} [°C]	p_{crit} [bar]	$p_{sat,15°C}$ [bar]	GWP_{100}	ASHRAE 34[b]	Type	No.
R1270 (Propene)	HC	91.1	45.6	8.9	3.1	A3	wet	1
R1234yf	HFO	94.7	33.8	5.1	0.501[a]	A2L	dry	2
R290 (n-Propane)	HC	96.7	42.5	7.3	0.02[a]	A3	wet	3
R161	HFC	102.1	50.1	7.0	4.84[a]	N/A	wet	4
R1243zf		103.8	35.2	4.4	0.261[a]	N/A	isentropic	5
R1234ze(E)	HFO	109.4	36.3	3.6	1.37[a]	N/A	isentropic	6
R152a	HFC	113.3	45.2	4.4	164[a]	A2	wet	7
R13I1		123.3	39.5	3.7	0.4	A1	wet	8
RC270 (cyclo-Propane)	HC	125.2	55.8	5.5	N/A	N/A	wet	9
RE170 (dimethyl-Ether)	HC	127.2	53.4	4.4	1.0	N/A	wet	10
R717 (Ammonia)		132.2	113.3	7.3	N/A	B2L	wet	11
R600a (iso-Butane)	HC	134.7	36.3	2.6	N/A	A3	dry	12
1-Butene	HC	146.1	40.1	2.2	N/A	N/A	dry	13
R1234ze(Z)	HFO	150.1	35.3	1.2	0.315[a]	A2L	isentropic	14
R600 (n-Butane)	HC	152.0	38.0	1.8	0.006[a]	A3	dry	15
trans-2-Butene	HC	155.5	40.3	1.7	N/A	N/A	dry	16
Neopentane	HC	160.6	32.0	1.2	N/A	N/A	dry	17
R1233zd(E)	HCFO	166.5	36.2	0.9	3.88[a]	A1	dry	18
Novec649		168.7	18.7	0.3	N/A	N/A	dry	19
R601a (iso-Pentane)	HC	187.2	33.8	0.6	N/A	A3	dry	20
R601 (n-Pentane)	HC	196.5	33.7	0.5	N/A	A3	dry	21
R602 (n-Hexane)	HC	234.7	30.4	0.1	3.1	N/A	dry	22
Acetone		235.0	47.0	0.2	0.5	N/A	isentropic	23
cyclo-Pentane	HC	238.6	45.7	0.3	N/A	N/A	dry	24
Methanol		239.4	82.2	0.1	2.8	N/A	wet	25
R603 (n-Heptane)	HC	267.0	27.4	<0.1	N/A	N/A	dry	26
cyclo-Hexane	HC	280.5	40.8	<0.1	N/A	N/A	dry	27
Benzene	HC	288.9	48.9	<0.1	N/A	N/A	dry	28
MDM	Siloxane	290.9	14.1	<0.1	N/A	N/A	dry	29
Toluene	HC	318.6	41.3	<0.1	3.3	N/A	dry	30
ethyl-Benzene	HC	344.0	36.2	<0.1	N/A	N/A	dry	31

[a] Value from Table 7.SM.7 of IPCC 6th Assessment Report (Smith *et al.*, 2021)
[b] ASHRAE Standard 34-2022, "Designation and Safety Classification of Refrigerants"